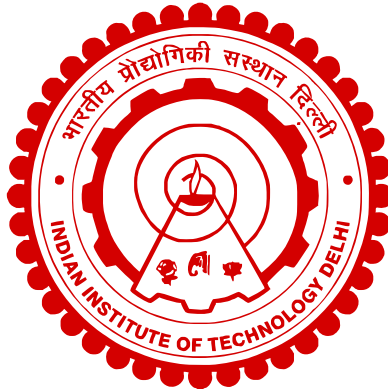


**ULTRASOUND-BASED HUMAN-MACHINE  
INTERFACES FOR CONTROL OF BIONIC  
DEVICES**

**ANNE TRYPHOSA KAMATHAM**



**Centre for Biomedical Engineering  
INDIAN INSTITUTE OF TECHNOLOGY DELHI**

**January, 2025**

© **Indian Institute of Technology Delhi (IITD), New Delhi, 2025**

**ULTRASOUND-BASED HUMAN-MACHINE  
INTERFACES FOR CONTROL OF BIONIC  
DEVICES**

*by*

**ANNE TRYPHOSA KAMATHAM**

**Centre for Biomedical Engineering**

*Submitted*

*in fulfillment of the requirements of the degree of Doctor of Philosophy*

*to the*



**INDIAN INSTITUTE OF TECHNOLOGY DELHI**

**January, 2025**

# CERTIFICATE

This is to certify that the thesis titled **Ultrasound-Based Human-Machine Interfaces for Control of Bionic Devices**, submitted by **Anne Tryphosa Kamatham**, to the Indian Institute of Technology, Delhi, for the award of the degree of **Doctor of Philosophy**, is a bonafide record of the research work done by her under our supervision and guidance. The contents of this thesis, in full or in parts, have not been submitted to any other Institute or University for the award of any degree or diploma.

**Dr. Biswarup Mukherjee**  
Assistant Professor  
Centre for Biomedical Engineering  
Indian Institute of Technology Delhi  
New Delhi-110016

New Delhi  
January, 2025

## ACKNOWLEDGEMENTS

Firstly, I am grateful to my supervisor, Prof. Biswarup Mukherjee, for the opportunity to learn under his guidance. I am forever thankful for his support, encouragement, advice, and, most importantly, for believing in me throughout my PhD journey. I am thankful for his valuable input in carrying out and accomplishing this work. I appreciate his patience and considerate demeanor toward his students, which immensely impacted my academic growth. I am thankful for his constant motivation to challenge myself as I grow as an independent researcher. I owe all my achievements during my PhD journey to him. I consider it an honor to have such a mentor to look up to.

I thank my student research committee members, Prof. Shouribratta Chatterjee, Prof. Ankesh Jain, and Prof Arnab Chanda, for their valuable input in improving my work.

I thank Prof. Srikumar V, professor at the Department of Physical Medicine and Rehabilitation, AIIMS, New Delhi, for helping me with the clinical validation and Dr. Jishnu for coordinating with the patients.

I thank the Ministry of Education, Government of India, for funding my research through the Prime Minister's Research Fellowship. The research grant allowed me to attend conferences crucial to my professional growth. It also helped me learn from the extensive teaching experience. I also thank the IEEE Instrumentation and Measurement Society for

the graduate fellowship award, which supported my research and to be a part of the IMS society.

This journey wouldn't have been enjoyable without the members of RISE lab who strived to maintain a supportive lab environment. I thank Manikandan and Kavita, who participated in many sonomyography discussions. Special thanks to Md.Adil for his expert contribution to the PCB design of OCTAvUS. I thank Ayesha, Vivek, Abhishek, Deep Roshan, Amit, Faiz, Chinmay, Joel, Swapnil, and Ria for sharing valuable technical and non-technical discussions and their support.

I thank my parents, K Yob and T S Grace Elizabeth, and my sisters, Dr. Pushpa Tryphena and Dr. Shiny Simon, for their prayers and unfailing support throughout my life.

Above all, I am deeply grateful to my Almighty God, whose knowledge is unfathomable. I am thankful to be bestowed with knowledge, understanding, strength, and patience to carry out this work and to have had all the blessings throughout my PhD journey. May this work be a blessing to the people in the days to come.

Anne Tryphosa Kamatham

---

## ABSTRACT

Upper limb loss can severely impede an individual’s ability to engage in daily activities. Although advanced multi-articulated prosthetic devices allow individuals to partially regain the functionality of lost limbs, the effectiveness of these devices relies on accurately sensing voluntary movement intent. Conventional surface electromyography’s (EMG) inability to capture voluntary activity from deeper muscle tissues and non-stationarity pose challenges in real-life prosthetic functionality. Recently, sonomyography (SMG) has been explored as an alternative to detect mechanical deformations of the muscle during dynamic voluntary activities using ultrasound (US). Using brightness-mode (B-mode) US systems, standard prosthetic control techniques such as gesture recognition and proportional control were successfully demonstrated. However, the size of the US systems must be significantly reduced, and relevant computational techniques must be developed to translate SMG for prosthetic applications. Therefore, this work presents a systematic approach to designing and developing wearable ultrasound systems and computational techniques for controlling upper limb prosthetic devices.

A computationally efficient Pearson’s correlation algorithm was used to quantify muscle activity from global features of the B-mode US images. Next, regression models and convolutional neural networks (CNN) were employed to demonstrate force prediction from highly sparse US images. An approach to extracting anatomically relevant features from sparse A-mode signals and a feature-free CNN, named SonoMyoNet, were proposed. A sys-

tematic analysis of the effects of sparsity on force prediction indicated that US data from eight channels could predict isometric force with accuracies  $> 90\%$  using regression models and  $> 94\%$  using SonoMyoNet. Based on the findings, A wearable 8-channel US system (OCTAvUS) and US transducers with optimized bandwidth were developed. OCTAvUS was uniquely configured to eliminate the RF signal frequencies at the hardware level, thereby obviating the need for high-speed digitization and reducing hardware complexity, storage, and communication requirements. The developed algorithms were evaluated in real-time in eight non-disabled individuals and two individuals with transradial amputation by conducting a real-time target achievement task involving proportional position control of multiple gestures. The non-disabled participants achieved average success rates of  $92.1\%$  whereas participants with amputation achieved average success rates of  $84.3\%$ .

This work systematically and comprehensively explores two critical aspects of SMG or ultrasound-based human-machine interfaces, particularly for controlling upper-extremity prosthetic devices. Firstly, the work presents a unique computational testbed for investigating the factors influencing the prediction accuracy of SMG-based joint kinematic prediction algorithms. The sparse representation and the analysis developed in this work lay the foundation for future ultrasound studies to leverage the outcomes for computationally efficient and translatable SMG systems. Secondly, these findings drive the development of a frugal and efficient wearable ultrasound-based muscle activity sensing hardware platform. This work also opens new avenues and research opportunities for wearable SMG-based systems in controlling assistive devices and investigations on understanding movement biomechanics involving dynamic activities.

**Keywords:** *Sonomyography, A-mode ultrasound, Wearable ultrasound, prosthetic control.*

---

## सार

ऊपरी अंग का नुकसान व्यक्ति की दैनिक गतिविधियों में संलग्न होने की क्षमता को गंभीर रूप से बाधित कर सकता है। हालाँकि उन्नत बहु-आर्टिकुलेटेड प्रोस्थेटिक डिवाइस व्यक्तियों को खोए हुए अंगों की कार्यक्षमता को आंशिक रूप से पुनः प्राप्त करने की अनुमति देते हैं, लेकिन इन उपकरणों की प्रभावशीलता स्वैच्छिक आंदोलन के इरादे को सटीक रूप से समझने पर निर्भर करती है। पारंपरिक सतह इलेक्ट्रोमायोग्राफी (EMG) की गहरी मांसपेशियों के ऊतकों से स्वैच्छिक गतिविधि को पकड़ने में असमर्थता और गैर-स्थिरता वास्तविक जीवन की कृत्रिम कार्यक्षमता में चुनौतियाँ पेश करती हैं। हाल ही में, अल्ट्रासाउंड (US) का उपयोग करके गतिशील स्वैच्छिक गतिविधियों के दौरान मांसपेशियों की यांत्रिक विकृतियों का पता लगाने के विकल्प के रूप में सोनोग्राफी (SMG) की खोज की गई है। ब्राइटनेस-मोड (B-मोड) सिस्टम का उपयोग करके, मानक प्रोस्थेटिक नियंत्रण तकनीक जैसे कि हावभाव पहचान और आनुपातिक नियंत्रण को सफलतापूर्वक प्रदर्शित किया गया। हालाँकि, US सिस्टम का आकार काफी कम किया जाना चाहिए, और प्रोस्थेटिक अनुप्रयोगों के लिए SMG का अनुवाद करने के लिए प्रासंगिक कम्प्यूटेशनल तकनीकों को विकसित किया जाना चाहिए। इसलिए, यह कार्य ऊपरी अंग प्रोस्थेटिक उपकरणों को नियंत्रित करने के लिए पहनने योग्य अल्ट्रासाउंड सिस्टम और कम्प्यूटेशनल तकनीकों को डिजाइन करने और विकसित करने के लिए एक व्यवस्थित दृष्टिकोण प्रस्तुत करता है।

बी-मोड यूएस छवियों की वैश्विक विशेषताओं से मांसपेशियों की गतिविधि को मापने के लिए एक कम्प्यूटेशनली कुशल पियर्सन के सहसंबंध एल्गोरिथ्म का उपयोग किया गया था। इसके बाद, अत्यधिक विरल यूएस छवियों से बल की भविष्यवाणी को प्रदर्शित करने के लिए रिग्रेशन मॉडल और कन्वोल्यूशनल न्यूरल नेटवर्क (CNN) का उपयोग किया गया। विरल A-मोड संकेतों से शारीरिक रूप से प्रासंगिक विशेषताओं को निकालने के लिए एक दृष्टिकोण और एक सुविधा-मुक्त CNN, जिसका नाम SonoMyoNet है, प्रस्तावित किया गया था। बल की भविष्यवाणी पर विरलता के प्रभावों के एक व्यवस्थित विश्लेषण ने संकेत दिया कि आठ चैनलों से यूएस डेटा रिग्रेशन मॉडल का उपयोग करके 90% से अधिक सटीकता के साथ आइसोमेट्रिक बल की भविष्यवाणी कर सकता है और SonoMyoNet का उपयोग करके 94% से अधिक सटीकता के साथ। निष्कर्षों के आधार पर, एक पहनने योग्य 8-चैनल यूएस सिस्टम (OCTAVUS) और अनुकूलित बैंडविड्थ वाले यूएस ट्रांसड्यूसर विकसित किए गए। OCTAVUS को हार्डवेयर स्तर पर

RF सिग्नल आवृत्तियों को समाप्त करने के लिए विशिष्ट रूप से कॉन्फ़िगर किया गया था, जिससे उच्च गति वाले डिजिटलीकरण की आवश्यकता समाप्त हो गई और हार्डवेयर जटिलता, भंडारण और संचार आवश्यकताओं को कम किया गया। विकसित एल्गोरिदम का वास्तविक समय में आठ गैर-विकलांग व्यक्तियों और ट्रांसरेडियल विच्छेदन वाले दो व्यक्तियों में कई इशारों के आनुपातिक स्थिति नियंत्रण से जुड़े एक वास्तविक समय लक्ष्य उपलब्धि कार्य का संचालन करके मूल्यांकन किया गया था। गैर-विकलांग प्रतिभागियों ने 92.1% की औसत सफलता दर हासिल की, जबकि विच्छेदन वाले प्रतिभागियों ने 84.3% की औसत सफलता दर हासिल की।

यह कार्य व्यवस्थित और व्यापक रूप से एसएमजी या अल्ट्रासाउंड-आधारित मानव-मशीन इंटरफ़ेस के दो महत्वपूर्ण पहलुओं की खोज करता है, विशेष रूप से ऊपरी-अंग कृत्रिम उपकरणों को नियंत्रित करने के लिए। सबसे पहले, यह कार्य एसएमजी-आधारित संयुक्त किनेमेटिक भविष्यवाणी एल्गोरिदम की भविष्यवाणी सटीकता को प्रभावित करने वाले कारकों की जांच के लिए एक अद्वितीय कम्प्यूटेशनल टेस्टबेड प्रस्तुत करता है। इस कार्य में विकसित विरल प्रतिनिधित्व और विश्लेषण कम्प्यूटेशनल रूप से कुशल और अनुवाद योग्य एसएमजी सिस्टम के परिणामों का लाभ उठाने के लिए भविष्य के अल्ट्रासाउंड अध्ययनों की नींव रखते हैं। यह कार्य सहायक उपकरणों को नियंत्रित करने और गतिशील गतिविधि से जुड़े मूवमेंट बायोमैकेनिक्स को समझने के लिए पहनने योग्य एसएमजी-आधारित प्रणालियों के लिए नए रास्ते और अनुसंधान के अवसर भी खोलता है।

**कीवर्ड:** सोनोग्राफी, ए-मोड अल्ट्रासाउंड, पहनने योग्य अल्ट्रासाउंड, प्रोस्थेटिक नियंत्रण।

# Contents

<b>CERTIFICATE</b>	<b>i</b>
<b>ACKNOWLEDGEMENTS</b>	<b>ii</b>
<b>ABSTRACT</b>	<b>iv</b>
<b>List of figures</b>	<b>xvi</b>
<b>List of tables</b>	<b>xvii</b>
<b>List of abbreviations</b>	<b>xviii</b>
<b>1 Introduction and Background</b>	<b>1</b>
1.1 Introduction . . . . .	1
1.2 Electromyography: From surface electrodes to implantable interfaces . . . .	4
1.2.1 Surface EMG-based myoelectric prosthetic control strategies . . . .	4
1.2.2 Invasive techniques for enhancing myoelectric control . . . . .	8
1.3 Ultrasound imaging-based muscle activity detection . . . . .	11
1.3.1 Sonomyography for prosthetic control . . . . .	13
1.3.2 Wearable A-mode ultrasound systems . . . . .	16
1.4 Research gaps . . . . .	19
1.5 Objectives of the research work . . . . .	20
<b>2 B-mode Ultrasound-based Muscle Activity Detection and Drift Compensation</b>	<b>22</b>
2.1 Introduction . . . . .	22
2.2 Experimental setup and methods . . . . .	24
2.2.1 Experimental paradigm . . . . .	25

---

2.2.2	Pearson's correlation-coefficient-based sonomyography signal . . . . .	26
2.2.3	Data preprocessing . . . . .	28
2.3	Dynamic characteristics of the sonomyography-based isometric force . . . . .	28
2.4	Static characteristics of sonomyography-based force measurement . . . . .	30
2.5	Conclusion . . . . .	32
<b>3</b>	<b>Feature-based Estimation of Isometric Force from Highly Sparse Ultra- sound Images</b>	<b>34</b>
3.1	Introduction . . . . .	34
3.2	Sparse sonomyography representation from B-mode ultrasound images . . . . .	34
3.3	Anatomically relevant A-mode signal feature extraction . . . . .	37
3.4	Regression models . . . . .	38
3.5	Isometric muscle force estimation . . . . .	41
3.6	Analysis of factors affecting force prediction performance . . . . .	42
3.6.1	Effect of the number of transducers (N) . . . . .	43
3.6.2	Effect of the placement location of transducers . . . . .	44
3.6.3	Effect of the number of peaks and peak width in A-mode signal . . . . .	44
3.6.4	Effect of speckle noise in ultrasound signals . . . . .	46
3.7	Conclusion . . . . .	48
<b>4</b>	<b>Feature-free Isometric Force Estimation from Sparse Ultrasound Im- ages</b>	<b>49</b>
4.1	Introduction . . . . .	49
4.2	SonoMyoNet architecture . . . . .	50
4.3	Analysis of the factors affecting force prediction accuracy . . . . .	52
4.4	Conclusion . . . . .	56
<b>5</b>	<b>Towards a Wearable Ultrasound Sensing System for Human-Machine Interfaces</b>	<b>58</b>
5.1	Introduction . . . . .	58
5.2	Wearable ultrasound system overview . . . . .	59
5.3	Design of wearable SMG sensor array . . . . .	59
5.3.1	Bandwidth characterization . . . . .	61
5.3.2	Impedance characterization . . . . .	63

---

---

5.3.3	Lateral resolution . . . . .	64
5.4	Design of wearable 8-channel multiplexed ultrasound transceiver system . .	65
5.4.1	Transmitter section . . . . .	65
5.4.2	Receiver section . . . . .	66
5.4.3	System functionality verification . . . . .	67
5.4.4	Signal to noise ratio . . . . .	67
5.4.5	Data acquisition . . . . .	67
5.5	Dynamic muscle activity detection - a pilot study . . . . .	69
5.6	Conclusion . . . . .	70
<b>6</b>	<b>Single Sonomyography Sensor-Based Hand Gesture Recognition Across Multiple Arm Positions</b>	<b>72</b>
6.1	Introduction . . . . .	72
6.2	Experimental setup and methods . . . . .	73
6.2.1	Experimental protocol . . . . .	73
6.2.2	Data processing . . . . .	74
6.3	Limb position affects on SMG gesture classification . . . . .	75
6.4	Conclusion . . . . .	77
<b>7</b>	<b>Wearable Ultrasound Sensing-Based Positional Proportional Control for Multiple Degrees-of-Freedom</b>	<b>79</b>
7.1	Introduction . . . . .	79
7.2	Experimental setup . . . . .	80
7.3	Generation of sparse ultrasound image frames from A-mode signals . . . .	81
7.4	Static characterization: Relationship between SMG signal and joint angles	82
7.5	Dynamic characterization: Proportional target achievement task . . . . .	85
7.5.1	Success rate . . . . .	86
7.5.2	Movement time . . . . .	88
7.5.3	Endpoint error and stability . . . . .	89
7.5.4	Path efficiency . . . . .	92
7.6	Validation with individuals with transradial amputation . . . . .	94
7.7	Conclusion . . . . .	99

---

<b>8 Limitations, Future Scope and Conclusion</b>	<b>100</b>
<b>References</b>	<b>113</b>
<b>Appendix</b>	<b>113</b>
<b>List of publications</b>	<b>117</b>
<b>Biodata</b>	<b>119</b>

## List of Figures

1.1	Penfield’s homunculus-A map of the somatomotor representation of upper limb and other body parts in the brain . . . . .	2
1.2	a) Body-powered prosthesis with a terminal grasper allows user control through tension on the harness transferred via contralateral shoulder movements; b) Bebionic hand by Ottobock, a multi-articulated prosthetic hand. . . . .	3
1.3	Surface Electromyography, the electrical activity in the muscles indicating neural activation can be measured by placing electrodes at the skin surface	5
1.4	The two popular myoelectric control strategies are a) Direct control and b) Pattern recognition. ( <i>Reproduced with permission from Springer Nature [1]</i> )	6
1.5	Invasive procedures for prosthetic integration a) implantable EMG electrodes (IEMS) [2] ( <i>Adapted with permission from Elsevier</i> ), b) Targeted muscle reinnervation [3] c) Osseointegration [4] ( <i>Adapted with permission from Wolters Kluwer Health, Inc.</i> ) . . . . .	11
1.6	Ultrasound imaging techniques. A-mode modality maps the amplitude of the echo intensities along depth as a 1-dimensional signal. M-mode is employed to visualize motion along a single scanline over a specified time interval. B-mode imaging allows visualization of cross-sectional areas at a specific time instant. . . . .	12
1.7	Various configurations of A-mode ultrasound systems designed to achieve wearability a) WMAUS [5] b) Miniaturized 4-channel system for prosthetic integration [6] c) WULPUS [7] d) TDS-based wearable ultrasound system [8].	17
2.1	Experimental setup showing the ultrasound probe, hand dynamometer, and an on-screen target achievement task. The dynamometer force output controls the on-screen user cursor, allowing the subject to follow the target. . .	23
2.2	a) Pearson’s correlation coefficient based on SMG signal generation. b) Polynomial detrending; and c) dynamic rest correction were used to compensate for the baseline drift. . . . .	27
2.3	Time series plots showing a) dynamometer force output, b) sonomyography signal and drift compensated sonomyography signal using c) polynomial detrending, and d) dynamic rest correction. . . . .	29

2.4	The relationship between normalized dynamometer force and sonomyography signals during a) contraction and b) relaxation phases for a representative subject. The sonomyography signal and measured dynamometer force had an inverse exponential relationship. . . . .	31
3.1	Generation of sparse ultrasound images. The intensities from sets of scanlines (columns) of the B-mode ultrasound images can be considered as A-mode signal intensities received by a single-element transducer. The average intensities indicate the A-mode envelope signals, which can be used as a one-dimensional signal or sparse ultrasound images. . . . .	35
3.2	A-mode signal feature extraction. The peaks and their locations indicate the presence of a target of anatomical relevance, and the mean and standard deviation indicate the size of the target . . . . .	37
3.3	Time series plot of one representative subject showing the true dynamometer force and the predicted force . . . . .	42
3.4	Effect of number of transducers on prediction accuracy. An increase in the number of scanlines and placement strategy significantly impacted the improvement in $R^2$ only when the number of transducers is $<4$ and had no effect when four or more transducers were used. . . . .	43
3.5	Effect of varying the number of peaks included from A-mode signal on the force prediction accuracy. The number of peaks had a statistically significant effect on the prediction accuracy. Gaussian procession regression model outperformed other models with $R^2$ of 0.98 with just one peak. . . . .	45
3.6	Effect of varying the ultrasound feature extraction window width on force prediction performance. The window width did not have a significant effect on the prediction accuracy. . . . .	46
3.7	Effect of speckle noise on force prediction accuracy. The regression models were trained with data uncorrupted by noise and tested with data corrupted with varying degrees of speckle noise variance. All models remain relatively unaffected by speckle noise levels up to 20 dB. . . . .	47
4.1	Architecture of the feature-free CNN, SonoMyoNet showing the sparse ultrasound image as input and force prediction output. The SonoMyoNet consists of three convolutional blocks of different filter sizes. Subject-specific training optimizes the number of convolutions to achieve the best predictions. . . .	50
4.2	Time series plot of SonoMyoNet predicted force and measured dynamometer force for one representative subject (S1). 9-fold cross-validation resulted in $R^2$ values $0.94 \pm 0.027$ , $0.93 \pm 0.045$ , $0.93 \pm 0.044$ for 4, 8, and 12 scanlines having a width of 4.4 mm width. . . . .	53
4.3	Effect of number of scanlines ( $N$ ) and scanline width ( $w$ ) on force prediction accuracy. $N = 4, 8,$ and $12$ scanlines and widths of $1.2$ mm, $2.8$ mm, and $4.4$ mm were considered. . . . .	54

4.4	a) Effect of scanline shift on $R^2$ . The SonoMyoNet was trained with images without shift and tested with data in which randomized scanlines shifts ranging from 0.4 mm to 2.4 mm were introduced. and b) Effect of speckle noise on $R^2$ . The SonoMyoNet was trained with speckle noise-free images and tested with images corrupted by speckle noise of different variances that degraded the image PSNR from 63 dB to 33 dB. The shaded area indicates the standard deviation. . . . .	56
5.1	Block diagram of the proposed wearable sonomyography system. The transmitter section consists of a high-voltage pulser and an analog switch, allowing eight-channel sequential operation. The receiver section is provided with the LNA-VGA and envelope detector, significantly reducing the hardware complexity of the conventional ultrasound systems . . . . .	59
5.2	a) The fabricated transducers with backing layer and electrical matching network b) The pulse-echo characterization setup consisted of an acrylic reflector in a container filled with water with transducers facing parallel to the reflector's surface. . . . .	60
5.3	(a) - (f) Plot showing the time domain and frequency domain responses for transducers without and with backing layer and matching network. g) The effect of the amount of tungsten powder on bandwidth and radial mode peaks. A bandwidth improvement and dampening of the radial mode vibrations were observed with an increase in Tungsten in the backing layer composition compared to an undamped transducer. . . . .	61
5.4	a) The magnitude and b) phase plots of the impedance characterization of the bare transducer, with backing, backing, and electrical matching. . . . .	63
5.5	a) The imaging capability of the transducer was characterized by imaging a 6 mm stainless steel rod phantom, b) a full-width half maxima of 2.3 mm was obtained with the fabricated transducers as opposed to c) standard transducer. . . . .	64
5.6	The hardware components used to implement the proposed wearable system. The image also shows the assembled wearable ultrasound system (OCTAvUS) and the power supply module. . . . .	66
5.7	High voltage excitation pulse, A-mode signal at LNA-VGA and A-mode envelope from the enveloped detector . . . . .	68
5.8	M-mode ultrasound data from a single channel during six different gestures acquired using the implemented system. . . . .	68
5.9	The eight-channel data recorded from a single participant was used to perform discrete classification using a linear discriminant classifier. Mean and standard deviation features were extracted from the A-mode envelope signals acquired in MATLAB . . . . .	70

---

6.1	Single channel ultrasound transducer was placed on the medial side of the forearm. Five gestures, namely, hand relaxed (HR), hand closed (HC), index point (IP), tripod grip (TG), and wrist rotation (WR), were performed at three limb positions: P1: arm at $90^0$ at the elbow, P2: arm downwards, and P3: arm raised overhead. . . . .	74
6.2	Classification accuracies for all the classifiers. The average classification accuracy was greater than 93% for all the classifiers. . . . .	76
6.3	Confusion charts of different classifiers. The charts show average ( $\pm$ standard deviation) inter and intra-class misclassifications at different limb positions for LDA and SVM with non-linear Gaussian kernel . . . . .	77
7.1	a) Experimental setup showing the user instrumented with a custom 8-channel SMG sensor connected to a commercial ultrasound pulser-receiver system and a virtual target achievement task. b) A-mode signal preprocessing, the preprocessed A-mode signals from all eight channels were arranged row-wise to form a sparse ultrasound frame. c) Generation of cursor control signal by quantifying the gesture position using Pearson's correlation coefficient. . .	82
7.2	Relationship between MCP joint angle and SMG signal for three gestures with the sensor array placed at proximal and distal locations on the forearm. Plots show the best $R^2$ values obtained for each gesture at each sensor position. .	83
7.3	The movement trajectories of a representative participant for a target presented at 0.6 achieved using all gestures. . . . .	85
7.4	Success rates achieved with different gestures at each position for three target widths. The participants achieved higher success rates with a target width of 15%. . . . .	87
7.5	Example of user trajectory and presented target. The outcome metrics, namely, movement time ( $T_m$ ), endpoint error, stability, path efficiency, and maximum velocity, were calculated from user trajectory. . . . .	87
7.6	Movement times achieved for different gestures for all target positions and target widths. A significant reduction in movement time can be seen when easier targets (15% target width) were presented. . . . .	88
7.7	Endpoint errors for each gesture at all target positions and widths. Endpoint errors were within 5% of the range. . . . .	90
7.8	Endpoint stability for each gesture at all target positions and widths. The standard deviation of the jitter was within 5% of the range. . . . .	91
7.9	Path efficiency of the user trajectories for all target positions and widths for all gestures. . . . .	93
7.10	Maximum velocity derived from the user trajectories for all target positions and widths for all gestures. Maximum velocity scaled linearly with target distance. . . . .	94

---

---

7.11	Success rates of two individuals with amputation for all four grasps. The participants achieved average success rates of 84 ( $\pm 5$ )% and an average movement time of 5.8 ( $\pm 2.3$ ) s across all gestures . . . . .	95
7.12	Endpoint error and endpoint stability at all target positions for all gestures. The average error and the standard deviation of the jitter was within 5% of the normalized range . . . . .	96
7.13	Path efficiency and maximum velocity derived from the user trajectories for all target positions for all gestures. Maximum velocity scaled linearly with target distance. . . . .	96

---

## List of Tables

1.1	B-mode ultrasound-based prosthetic control strategies . . . . .	14
1.2	Existing wearable A-mode systems . . . . .	17
1.3	A-mode signal features . . . . .	18
2.1	Demographics of study participants . . . . .	24
2.2	Inverse-exponential model fitting coefficients $a, b$ , and $c$ (mean $\pm$ standard deviation) and $R^2$ values for all the subjects . . . . .	32
4.1	Comparison of SonoMyoNet with Regression models . . . . .	55
5.1	Impedance characteristics of the fabricated transducer . . . . .	64
7.1	Mean and standard deviation of $R^2$ values obtained for each gesture at proximal and distal positions across all subjects . . . . .	84
7.2	Comparison of existing EMG and SMG-based proportional control strategies with this work . . . . .	92
7.3	Demographics of transradial amputees . . . . .	95
7.4	Comparison of average outcome metrics of non-disabled and trans-radial amputee individuals . . . . .	98
7.5	Comparison of average outcome metrics of individuals with transradial amputation . . . . .	98

## List of abbreviations

EMG	Electromyography
DOF	Degree of freedom
SMG	Sonomyography
A-mode	Amplitude-mode
M-mode	Motion-mode
B-mode	Brightness-mode
PZT	Lead zirconate titanate
PVDF	Polyvinylidene fluoride
MVIC	Maximum Voluntary Isometric Contraction
CNN	Convolutional Neural Network
PRF	Pulse repetition frequency
LNA	Low noise amplifier
VGA	Variable gain amplifier
TGC	Time gain compensation